Effect of Oxygen Termination on the Interaction of First Row Transition Metals with M_2C MXenes and the Feasibility of Single-Atom Catalysts†

Masoomeh Keyhanian,[1,2] Davood Farmanzadeh,[2] Ángel Morales-García[1,*] Francesc Illas,[1]

[1]*Departament de Ciència de Materials i Química Física & Institut de Química Teòrica i Computacional (IQTCUB), Universitat de Barcelona, c/Martí i Franquès 1-11, 08028 Barcelona, Spain*

[2]Department of Physical Chemistry, Faculty of Chemistry, University of Mazandaran, Babolsar 47416-95447, Iran

Abstract

A density functional theory-based study is performed to investigate the stability of single atom catalysts (SACs) over a series of O-terminated MXenes with stoichiometry M_2CO_2. To this purpose, we select the first-row transition metals as adatoms and nine MXene surfaces as supports. From a thermodynamic viewpoint, the stability of the resulting SACs is favorable for all combinations between adatoms and MXenes. However, the adatoms trends to cluster together to a rather low energy barrier for diffusion promote largely affect their stability. The present systematic study shows that Sc@ and Ti@M_2CO_2 are the most feasible SACs because of the high metal-support interaction, the low trend to form metal clusters and the high diffusion barriers. The present results could be useful to experimentalists aiming at synthetizing SACs based on MXenes.

*Corresponding author: angel.morales@ub.edu

† Electronic supplementary information (ESI) available: Tables that compile adsorption energies, structural parameters, charge transfer, difference between the adsorption energy and the cohesive energy, and barrier energies of all M@M_2CO_2. Fitting parameters of E_{ads} (TM@M_2C) vs. E_{ads} (TM@M_2CO_2) are listed in Table S10.

1. INTRODUCTION

The term of single-atom catalysts (SACs) was first introduced a decade ago and nowadays constitutes a fundamental piece in the search for improvements in heterogeneous catalysis, and electrocatalysis.[1-4] SACs involved dispersed atoms anchored over a solid substrate sufficiently spatially separated to minimize their lateral interactions and to allow their interaction with the desired reactant.[5] There is strong evidence that such arrangements can provide efficient and highly active surfaces sites for catalytic transformations under mild conditions. Indeed, the presence of isolating active atoms not only maximizes the number of active sites but also increases efficiency, reduces the load of noble metals (*e.g.*, Ru, Rh, Pt, Pd, Ni, Co, Au, and Ag) and, compared to conventional catalysts, may significantly enhance the catalytic selectivity.[6-11] In other words, the attainment of an optimal utilization and efficiency is highly related to the number of isolated atoms that act as active sites. Hence, one of the existing challenges towards a more sustainable chemical industry is precisely to find out suitable supports over which single atoms may be anchored without sintering. Efficient supporting frameworks not only have to facilitate anchoring of individual atoms. In fact, the ideal support must also firmly accommodate them to prevent sintering during the catalytic process. Clearly, a systematic search beyond trial and error would help to optimize the loading and scale up synthesis leading to efficient SAC technology.[12]

Metal oxides such as FeO_x,[1] CeO_2,[13] Al_2O_3,[14] and ZnO[15] have been experimentally and/or theoretically probed as very promising supports for SACs. Often, their role in the catalytic conversion goes beyond stabilizing single atoms and actively participate in the reactions. Metal surfaces have been also used to stabilize isolated adatoms, but their use is scarce.[16,17] More recently, the blooming of newly developed 2D materials has provided new types of supports with significant improvements in the performance of SACs. In addition to graphene,[18] other 2D layered materials have emerged as anchors for single atoms such as transition metal dichalcogenides (TMDs), and layered double hydroxides (LDHs).[1920,] More recently, the appearance of a new class of 2D carbides and/or nitrides materials known as MXenes[21] has opened new avenues in heterogeneous catalysis, in general,[22] and SACs in particular.[23-25]

MXenes are structurally described by the $M_{n+1}X_nT_x$ general formula where n=1-3; M is early transition metal— typically Sc, Ti, Zr, Hf, V, Nb, Ta, Cr, Mo and W—; X stands for C or N; and T_x corresponds to the surface terminations— most often O, H, OH, or F). They are regularly synthetized from the precursor MAX phases with general formula $M_{n+1}AX_n$, where A represents

elements from the groups 13 and 14 of the periodic table.[21] By using a selective chemical etching procedure, M–A bonds are dissembled generating MXene nanosheets.[26] The etching agent employed during this structural disassembly determines the functionalization (T_x) of MXene surfaces. Note that these materials have gained immense attention during last decade for technological applications because they possess hydrophilic surfaces and high metallic conductivities that make them appropriate for energy storage devices, electromagnetic interference shielding, conducting thin films to name a few.[27]

The performance and possible use of MXenes in catalysis have been the object of two recent reviews.[22,28] Particularly, these materials have exhibited promising results in electrocatalysis for relevant reactions such as hydrogen evolution reaction (HER),[29,30] overall water splitting (OWS),[31] nitrogen reduction reaction (NRR),[32,33] and oxygen reduction reaction (ORR).[34] Similar encouraging results have been reported in heterogeneously catalyzed processes posing MXenes as feasible catalyst to active and dissociate H_2O[35] and the highly stable CO_2 and N_2 molecules.[36,37] These experimental and theoretical investigations evidence a promising new avenue in catalysis based on MXene-derived materials.[22] Given that transition metal carbides behave as active supports for metallic nanoparticles[38] and metal adatoms,[39] to the point to activate methane at room temperature,[40] one may wonder about the possibility of using MXenes as a suitable support precisely for confining and stabilizing single atoms. Indeed, single Pt atoms have been immobilized on defective $Mo_2TiC_2T_x$ MXene showing an efficient performance for HER.[41] Furthermore, first-principles calculations predicted that single Zn atoms can be anchored favorably over defective V_2CO_2 nanosheets showing a good performance toward the CO oxidation.[42] In addition, single Ni atoms over Ti_2NO_2 catalyst emerge as suitable SACs for NRR.[43] More recently, a combined theoretical and experimental study introduced a SAC composed of single cobalt atoms linked to $Ti_3C_2T_x$ which is active for CO_2 photoconversion under VIS-light.[44] Apart from these studies, the literature of single-atoms anchored on MXenes is scarce and mostly limited to a systematic computational analysis studied the structural and electronic properties of the late metals of a series 3*d*, 4*d*, and 5*d* metals anchored on bare Ti_3C_2,[45] and a more systematic study by some of us analyzing in detail the interaction of first row transition metals with a series of bare M_2C (M=Ti, Zr, Hf, V, Nb, Ta, Cr, Mo, and W) MXenes.[25] Clearly, further studies are required to capture systematic trends by analyzing a series in the periodic table. Nevertheless, these two studies focus on bare MXenes which, while some have been experimentally prepared, removing

the termination involves quite complicated and costly post-synthesis heating treatments.[46] On the other hand, MXenes with just an O-termination are easier to prepare. [47] Thus, in the present study, we move a step forward by analyzing the possibility of SACs formation over O-terminated MXenes (M_2CO_2). Thus, a systematic study based on first-principles calculations similar to the one reported for bare M_2C MXenes[25] has been undertaken. In the present work, we report the results of such a detailed investigation including predicting trends in structural, energetic, and bonding properties, plus adsorption characteristics, and diffusion barriers of the first-row transition metals on M_2CO_2 (M=Ti, Zr, Hf, V, Nb, Ta, Cr, Mo, and W) MXenes. In addition, we further compare the possibility to obtain SACs supported on either bare or O-terminated MXenes which helps to clarify how the oxygen functionalization affects the formation of SACs based on MXenes.

2. COMPUTATIONAL METHODS AND MODELS

The interaction between the 3*d* transition metal atoms and the basal surface of the M_2CO_2 (M=Ti, Zr, Hf, V, Nb, Ta, Cr, Mo, and W) series of MXenes has been studied by means of periodic density functional theory (DFT) based calculations including spin polarization. All calculations were carried out using the Vienna *Ab Initio* Simulation Package (VASP)[48,49] in which the Kohn-Sham equations are solved using a plane-wave basis, with energy cutoff of 415 eV, to represent the valence electron density and the effect of the atomic cores on the valence electrons is accounted for through the Projector Augmented Wave (PAW) method developed by Blöchl.[50] The numerical integrations in the Brillouin zone were performed using a 5×5×1 Monkhorst-Pack grid of special **k**-points.[51] The broadly used Perdew–Burke–Ernzerhof (PBE)[52] variant of the generalized gradient approximation (GGA) was chosen to represent the exchange-correlation density functional. To overcome the limitations of standard DFT methods to describe weak interactions, the Grimme's D3 method[53] has been considered to account for dispersion. The structural optimizations were considered converged when the residual Hellmann–Feynman forces acting on the atoms were below 0.01 eV $Å^{-1}$. The total energy convergence was set to 10^{-5} eV/atom.

The M_2CO_2 MXenes were represented by means of a *p*(3 x 3) slab supercell which ensures negligible interaction between the supported single atoms in the periodic images. The optimized unit cell of the bare MXene in the ABC stacking inherited from the MAX phase is always used. For the O terminating layers, O atoms are placed in the possible three-folds sites as indicated in Figure 1. These lead to two different stackings relative to the ABC one of the MXenes that are denoted as CABCA and BABCB, respectively, as shown in Fig. 1. Similar models were used in

previous work analyzing the effect of O-terminations on the core level binding energy shifts in these systems.[54] Furthermore, a 16 Å vacuum along the *c*-axis was selected to ensure that the interaction between replicated slabs is negligible. The interaction between the transition metal atoms and O-terminated MXene carbides with M_2CO_2 is established from the calculated adsorption energy, E_{ads}, which is defined as:

$$E_{\text{ads}} = -[E_{\text{TM@MXene}} - (E_{\text{MXene}} + E_{\text{TM}})] \quad (1)$$

where $E_{\text{TM@MXene}}$, E_{MXene}, E_{TM} stand for the total energies of the MXene supercell with the adsorbed TM adatom, the clean M_2CO_2(0001) surface, and the isolated TM atom, respectively. The energy of the isolated TM atom has been obtained by placing it in a large enough asymmetric box and including spin polarization, as previously reported.[55] According to the definition in Eq. (1), the more positive E_{ads} implies the stronger the interaction between the MXene and the TM adatom. Further information regarding the chemical interaction is obtained from the topological Bader charges,[56] providing also the amount of electron transfer between the M_2CO_2(0001) MXenes and SAs.

To estimate the character, isolating or clustering, of the adsorbed single atoms, we rely on the energy difference (E_{diff}) between the adsorption energy (E_{ads}) and the cohesive energy of the bulk metal (E_{coh}) per atom as in Eq. (2)

$$E_{\text{diff}} = E_{\text{ads}} - E_{\text{coh}} \quad (2)$$

where E_{coh} is defined as

$$E_{coh} = E_{\text{TM}} - \frac{E_{\text{TM(bulk)}}}{N} \quad (3)$$

where E_{TM} is as in Eq. (1) and $E_{TM(bulk)}$ denotes the energy of the corresponding transition metal crystal containing *N* atoms in the unit cell. According to Eq. (2), $E_{diff} > 0$ —or equivalently $E_{ads} > E_{coh}$ —implies that the isolating behavior is favorable; whereas $E_{diff} < 0$ (*i.e.*, $E_{ads} < E_{coh}$) indicates that clustering will be thermodynamically favored. To investigate possible kinetic restriction for clustering, the diffusion barrier for the adsorbed atom moving from one active site to an equivalent empty one was also scrutinized. This considered all the different nonequivalent pathways for the single atoms diffusion across the M_2CO_2(0001) MXene surfaces. The minimum energy path (MEP) was established by considering a series of structural images leading from the initial to final structures, leading also to locate the corresponding transition state (TS). To perform this analysis,

the bottom oxygen layer of the M_2CO_2(0001) MXene surface and with the position of the TM adatom in the plane were fixed while, for each position, the vertical distance to the MXene surface was optimized. This simple constrained search guarantees finding the MEP for the diffusion process. Nevertheless, the TS is fully characterized by vibrational analysis. Finally, the energy barrier for diffusion (E_{bar}) obtained was estimated as the difference between the energy of the TS and of the most stable adsorption sites. Note that a similar strategy was employed in previous studies of some of us.[25]

3. RESULTS AND DISCUSSION

3. 1. Stability of TM adatoms on M_2CO_2 MXenes

Before adsorbing TM adatoms over O-terminated MXenes, we analyze in detail the structure of O-terminated M_2C MXene surfaces. From a structural viewpoint, MXenes show two hollow sites labeled as face-centered cubic (*fcc*) and hexagonal close-packed (*hcp*) where O atoms can anchor (Fig. 1). Both sites, *fcc* and *hcp*, are explored in all MXene surfaces to identify the appropriate arrangements described with the CABCA and BABCB stackings. The former is favorable in those MXenes composed of metals from d^2-(Ti, Zr, Hf) and d^3-(V, Nb, Ta) metals, and d^4-(Cr).[54] On the other hand, we find that the MXenes composed of d^4-(Mo, W) metals prefer the BABCB stacking which is consistent with previous studies.[57-59] Here, we note that Tan *et al*.[59] claimed that the BABCB stacking was preferred for Cr_2CO_2. A result that may come from the use of a different functional (DFT+*U* with *U*=4 eV) to initially optimize the crystal structures that were later refined with a hybrid density functional. Indeed, the energy difference between both stackings is less than 0.1 eV per unit of Cr_2CO_2 using our computational strategy which is within the accuracy of the present density functional calculations. Finally, one must also point out that a different ABA stacking is possible for the MXene central layers which sometimes is more favorable than the one inherited from the MAX phase and may have impact on the properties of the adsorbed molecules.[60,61] In the present work, only the ABC stacking of the M_2C MXenes is considered.

Once we have identified the suitable stacking of each M_2C MXene, we proceed to investigate the binding strength corresponding to the interaction between the first series of transition metals of the periodic table (Sc, Ti, V, Cr, Mn, Fe, Co, Ni, Cu, and Zn) and the O-terminated MXenes. Analyzing the topology of the O-terminated M_2C(0001) MXene surfaces, there are four sites where TM adatoms can be adsorbed. Starting with the ABCAB stacking (see Fig. 1, bottom panel), one finds the top (T) site where the TM adatom is located directly on the top

of O atom; the bridge (B) site where the TM adatom places over the midpoint of the M–O bond; the carbon hollow (H_C) site; here, the TM adatoms is in a hollow site around three oxygen atoms and its position matches with the C atom three atomic layers below. Finally, the empty hollow (H_e) site is where the TM adatom is in another hollow site matching its position with the O atom located five layers below (see Fig. 1b). T, B and H_e sites are also found on MXene surfaces with the BABCB stacking together with a new hollow site labeled as E, which locates on the TM adatom matching with a M atom four layers below (see Fig. 1, bottom panel).

Although TM adatoms were initially placed on all above-described sites, the H_C and H_e hollow sites emerged as the ones featuring a more favorable interaction, the geometry optimization always converging to these structures, irrespective of the starting point. The systematic study predicts that the H_C site is the preferred on for Ti, Zr, Hf, V, Nb, and Ta preferential over the M_2CO_2(0001) MXene surface with the exception of Co, Ni, and Cu single atoms on V_2CO_2 MXenes that prefer the H_e site, and Zn at Nb_2CO_2 which prefers the B site. On the other hand, the interaction of TM single atoms with Cr_2CO_2, Mo_2CO_2, and W_2CO_2 MXene substrates is more favorable when these are placed directly above the E and H_e sites (Further details can be found in the ESI†).

From the trends of the adsorption energies depicted in Fig. 2, one concludes that the interaction of all TM adatoms is energetically favorable as in all cases $E_{ads} > 0$, *cf.* Eq. (1). Nevertheless, E_{ads} spans a broad range of 0.5 and 10 eV. To rationalize this energetic spectrum, we analyze the stability of isolated TMs as a tentative initial guide. The early transition metals (*i.e.*, Sc, Ti, and V) expose the largest E_{ads} above 3.8 eV regardless the MXene composition. We can establish a bottom limit at ~4 eV and a top limit above ~8 eV that correspond to Hf_2CO_2 and Cr_2CO_2 MXenes, respectively. The interaction energies of these early TMs with the rest of MXenes are somewhere in the middle of the range defined by these limits (Fig. 2). The reason for this large interaction is attributed to the low number of *d* electrons of TM adatoms. Following this argument, one readily sees

that E_{ads} decreases with increasing number of *d* electrons. In other words, the interaction energy decreases as moving along the series. The semi or full occupancy of *d* orbitals tends to stabilize the isolated TM adatoms promoting lower E_{ads} with the O-terminated MXene surfaces. This is the reason why E_{ads} drops notoriously when Cr (d^5) or Zn (d^{10}) adatoms are anchored on MXenes. Interestingly, similar trends have been observed over the adsorption of the same TM

adatoms on bare MXenes, and carbon-derived substrates.[25,62,63] In this sense, the presence of the O-termination does not seem to represent a big change relative to the bare MXenes.

In principle, one may assume that the trend observed on E_{ads} correlates with the electron transfer. To clarify this issue, Atom-in-Molecules (AIM) theory[56] is employed to understand the trends observed for the interactions in terms of chemical concepts by quantifying the degree of charge transfer between both systems. The charge transfer (ΔQ) is positive in all cases (see Fig. 3), the TM gets oxidized as the electron density is transferred from the TM adatom towards the MXene. The results in Fig. 3 confirm that ΔQ decreases moving along the series as E_{ads} decreases. The case of Zn adatom is particularly interesting because ΔQ varies significantly. To shed light on the behavior of this TM adatom, we analyze the vertical distance (h) between TM adatom and the O-terminated MXene surface. Fig. 4 shows the evolution of h along the d series. Such vertical distance varies in the 0.5–1.5 Å range for all TM adatoms except for Zn adatom. In this case, the O-terminated MXene surfaces receiving more electrons from Zn adatoms are those where the vertical distance is small (*i.e.*, V_2CO_2, Cr_2CO_2, Mo_2CO_2, and W_2CO_2), whereas a large h correlates with low ΔQ thus suggesting that the interaction between TM atoms has two main origins, the redox process and the resulting strong electrostatic component. This is clear from Fig. 5 where E_{ads} is plotted versus ΔQ for all the considered systems. The correlation is not perfect which indicates that charge transfer is not the only contribution to the bonding between the TM and the M_2CO_2 MXenes; yet the trend is clear and provides evidence that this is a dominant effect.

3. 2. Isolating stability and diffusion barriers

Results from the previous section indicate that the formation of SACs based on O-terminated MXenes can be energetically possible and we have rationalized the trends through some chemical and structural descriptors. As commented in the previous section, the comparison between E_{ads} of TM adatoms on MXenes and the cohesive energy of bulk metals allows us to discern whether SACs formation is energetically favored (E_{diff} >0 or $E_{ads} > E_{coh}$) or if, on the contrary, clustering would prevail ($E_{diff} < 0$ or $E_{ads} < E_{coh}$); the relevant results are summarized in Table 1.

The final E_{diff} value depends in part on the TM adatom and on the MXene where is anchored because E_{ads} is structural-dependent as shown its trend in Fig. 2. According to the present results, Sc and Ti adatoms are the plausible metals to form potential SACs based on MXenes because they expose high adsorption energies that favor the isolating with E_{diff} values above 0.60

eV (Table 1). In addition, we predict that the Cr_2CO_2(0001) MXene surface constitutes a potential MXene substrate to form SACs as, for this MXene, Sc, Ti, V, Cr, Mn, and Zn adatoms exhibit E_{diff} >0 and, consequently, isolating is energetically favorable with respect to clustering. It is worth noting that, while E_{diff} provides a thermodynamic guide for the formation of SACs, there are many cases where E_{diff} < 0 eV and clustering of TM adatoms will be, in principle, favorable although this may be hindered by large energy barriers for diffusion. To address this issue, we investigate the energetics of the diffusion of TM adatoms from site to site on the MXene surface focusing essentially on the diffusion energy barriers (E_{bar}).

Fig. 6 shows the possible diffusion paths analyzed on the MXene surfaces with CABCA and BABCB stackings. Different hollow-to-hollow paths along MXene surfaces are investigated in which the most suitable structures of TM@MXene have been considered as the initial state and final state to obtain the lowest E_{bar}. Starting with the CABCA stacking and since the preferred site above M_2CO_2(0001) MXene is the H_C one, three possible pathways are possible defined as path 1: $H_C \rightarrow H_e \rightarrow H_C$, path 2: $H_C \rightarrow B \rightarrow H_C$, and path 3: $H_C \rightarrow T \rightarrow H_C$ being the lowest energy barrier obtained through the former one. Also, because the H_e and E sites are preferred for single TM atoms above the BABCB stacking, we explored different kinds of pathways, as presented in the right part of Fig. 6, and considered various possible diffusion paths including path 1: $H_e \rightarrow E \rightarrow H_e$, path 2: $H_e \rightarrow h_3 \rightarrow H_e$, and path 3: $H_e \rightarrow T \rightarrow H_e$ for the preferred H_e site. Here, the former path shows the lowest energy barrier. In addition, path 1: $E \rightarrow T \rightarrow E$, path 2: $E \rightarrow B \rightarrow E$, and path 3: $E \rightarrow H_e \rightarrow E$ for the preferred E site were analyzed showing the later one the lowest energy barrier. Note that in the h_3 site the TM adatom is located above the midpoint of the O–M bond in lower layer. Table 2 summarized the lowest E_{bar} values. There, Sc, Ti and V adatoms feature the largest E_{bar} values which are connected with the largest E_{ads} values too (see Fig. 2). On the other hand, Zn@MXenes have the lowest E_{bar} which is, again, connected with the lowest E_{ads} (see Fig. 2) except for Zn@Cr_2CO_2 where its E_{diff} = 0.56 eV correlates with its E_{bar} = 0.71 eV. To clarify the interplay between E_{diff} and E_{bar} we focus on Sc@Hf_2CO_2, Ti@Ta_2CO_2, Fe@V_2CO_2, and Co@Cr_2CO_2 systems. According to the thermodynamic criteria, all these SACs are unfeasible because E_{diff} < 0 eV (*i.e.*, -0.32, -0.78, -1.06, and -0.80 eV respectively) and the TM adatoms will tend to form metal clusters on the O-terminated MXene surfaces. Interestingly, such clustering formation is likely to be inhibited by a large E_{bar} above 1 eV (*i.e.*, 1.15, 1.48, 1.34, and 1.30 respectively). This indicates that a relatively high thermal activation is required to initiate the

diffusion along the MXene surface. In short, low clustering energies coupled with high diffusion energy barriers could generate suitable SACs based on MXenes. Indeed, such SACs could be appropriate for some catalytic reactions on which the operating temperature does not overcome the thermal activation required to form clusters. Clearly, additional work is needed to investigate the performance of a given O-terminated MXene based for a particular chemical reaction of interest which is out of the scope of the present work.

3. 3. Bare (M_2C) *versus* O-terminated (M_2CO_2) MXenes

A previous study performed by some of us[25] reported the suitability of bare MXene carbides with stoichiometry M_2C as platforms to generate SACs. Here an interesting comparison emerges when analyzing E_{ads} for TM on bare and O-terminated MXene carbides as shown in Fig. 7. We want to note that we focus on trends although linear regressions analysis is listed in Table S10 of the ESI. Nevertheless, the correlation factor (R^2) is too small to be taken from a quantitative point of view. Yet, its value increase as moving along the *d* series. Taking as example Ti-, V-, and Cr-derived MXenes, their corresponding R^2 are 0.42, 0.54, and 0.74. Similar trends are systematically obtained for the rest of MXenes. This allows one to select the appropriate MXene substrate (bare or O-terminated) for anchoring TM adatoms, at least based on the thermodynamic criteria.

Analyzing the MXenes that show the largest R^2 (*i.e.*, Cr-, Mo-, and W- derived ones) and the linear fitting (see Table S10), the interaction of the TM atoms with bare MXenes is larger than with their O-terminated counterparts. This conclusion is quite general even if, depending on the composition, each MXene surface has to be considered to extract further conclusions. In short, the interaction of first row TM atoms with O-terminated MXenes is weaker than with bare MXenes but yet sufficient to maintain TM adatoms anchored to the surface. This is in line with findings from two recent computational studies on $Ti@Zr_2CO_2$, $Sc@Zr_2CO_2$ and $Pt@M_2CO_2$.[65,66]

CONCLUSIONS

The interaction of TM adatoms with O-terminated MXenes, (M_2CO_2, M=Ti, Zr, Hf, V, Nb, Ta, Cr, Mo, and W) was investigated using first-principles calculations and periodic models. Thermodynamic and kinetic aspects were analyzed in detail based on different energetic criteria. The interaction strength measured by the adsorption energy (E_{ads}) is rather large for all investigated TM adatoms regardless of the MXene substrate. The largest interaction is observed in the early-

TM adatoms, and it goes down when moving along the *d* series. Importantly, the anchoring of a TM adatoms is favorable on all MXene substrates analyzed. This interaction is coupled with a systematic charge transfer from the TM adatom toward MXene. This implies that the largest interaction promotes the largest charge transfer and vice versa. Finally, a structural descriptor as the vertical distance between TM adatom and MXenes is also connected with E_{ads} and the charge transfer showing that a small distance is associated with large E_{ads} and the charge transfer.

In addition, comparing the adsorption and cohesive energy provides information regarding whether the formation of metal clusters is or not favored with respect to the situation involving well separated, isolated, metal adatoms. The analysis of the energy profile involved in adatom diffusion, a necessary step towards clustering, complements the thermodynamic picture adding the kinetic viewpoint. From the resulting data, it is concluded that Sc and Ti adatoms are likely to be favorable in the majority of MXene platforms due to the isolating adatom is favorable and a large diffusion barrier guarantees the stability of such SACs. In short, we conclude that large adsorption energies and charge transfers connected with a low capacity to form metal clusters and a high diffusion barrier of the TM adatom guarantees the feasible design of SACs based on MXenes. Furthermore, even for those TM adatoms where the formation of metal cluster is favored, the sintering process can be inhibited by relatively large diffusion barriers. These energetic descriptors may be useful for experimentalisst and our study goes beyond MXenes and can be employed to analyze any SACs with any material as potential substrates.

Finally, the comparison of E_{ads} between bare M_2C and O-terminated M_2CO_2 offers some interesting differences. Overall, the interactions between the TM atoms and the MXene substrates are larger for the bare ones although the presence of O layers does not largely affect the main trends. Nevertheless, it is worth pointing out that Sc and Ti adatoms are the most suitable metals to form SACs over M_2CO_2, whereas Zn adatoms are the preferential ones over M_2C. Therefore, one can speculate that functionalization may provide a tool to possibly control and select the desired transition metal to synthesize SACs supported on MXenes.

ACKNOWLEDGEMENTS

The research reported in this work has been supported by the Spanish MICIUN RTI2018-095460-B-I00 and María de Maeztu MDM-2017-0767 grant and, in part, by COST Action CA18234. A. M.-G. thanks to Spanish MICIUN for a Juan de la Cierva (IJCI-2017-31979).

Fig.1 Top and side views of bare MXene structure with stoichiometry M_2C and ABC stacking (top panel) and of the O-terminated MXenes with CABCA and BABCB stacking (bottom panel). The red dashed lines and circles labeled with digits 1, 2, and 3 corresponds to top (T), hexagonal close-packed (hcp), and face-centered cubic (fcc) sites. On the side views, the anchored sites for TMs are depicted in purple. Green, brown, and red spheres correspond to transition metal, carbon, and oxygen atoms, respectively.

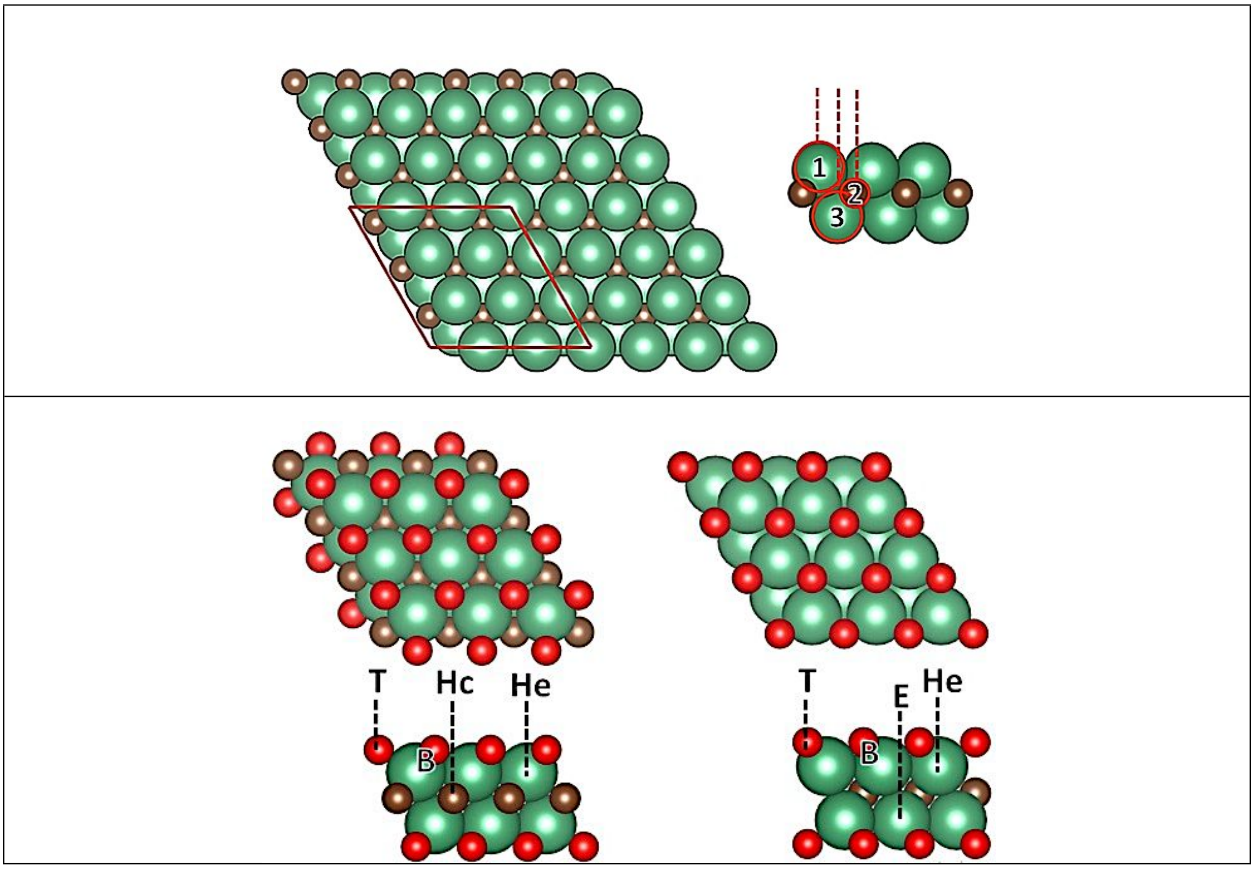

Fig. 2 Adsorption energy (E_{ads}) of 3*d* TM adatoms on the M_2CO_2(0001) MXene surfaces. The most favorable E_{ads} at PBE-D3 configurations have been selected for each M@M_2CO_2 regardless the adsorption site (see ESI).

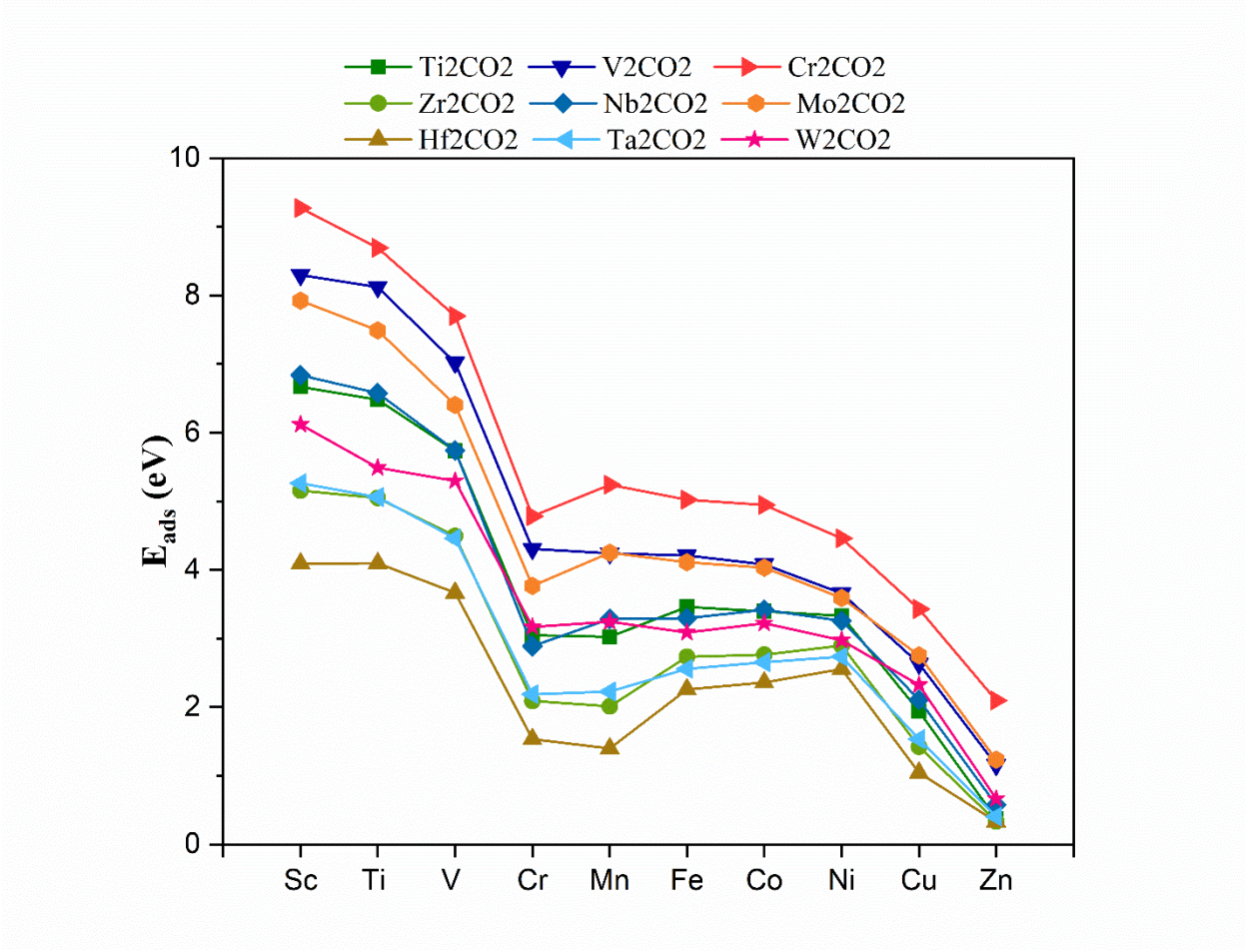

Fig. 3 Electron transfer (ΔQ) induced by the interaction of TM adatoms with O-terminated MXenes. These results correspond to the most favorable situations at PBE-D3 shown in Fig. 2. Noting that ΔQ > 0 corresponds to an electron transfer from the TM adatom towards MXene substrate.

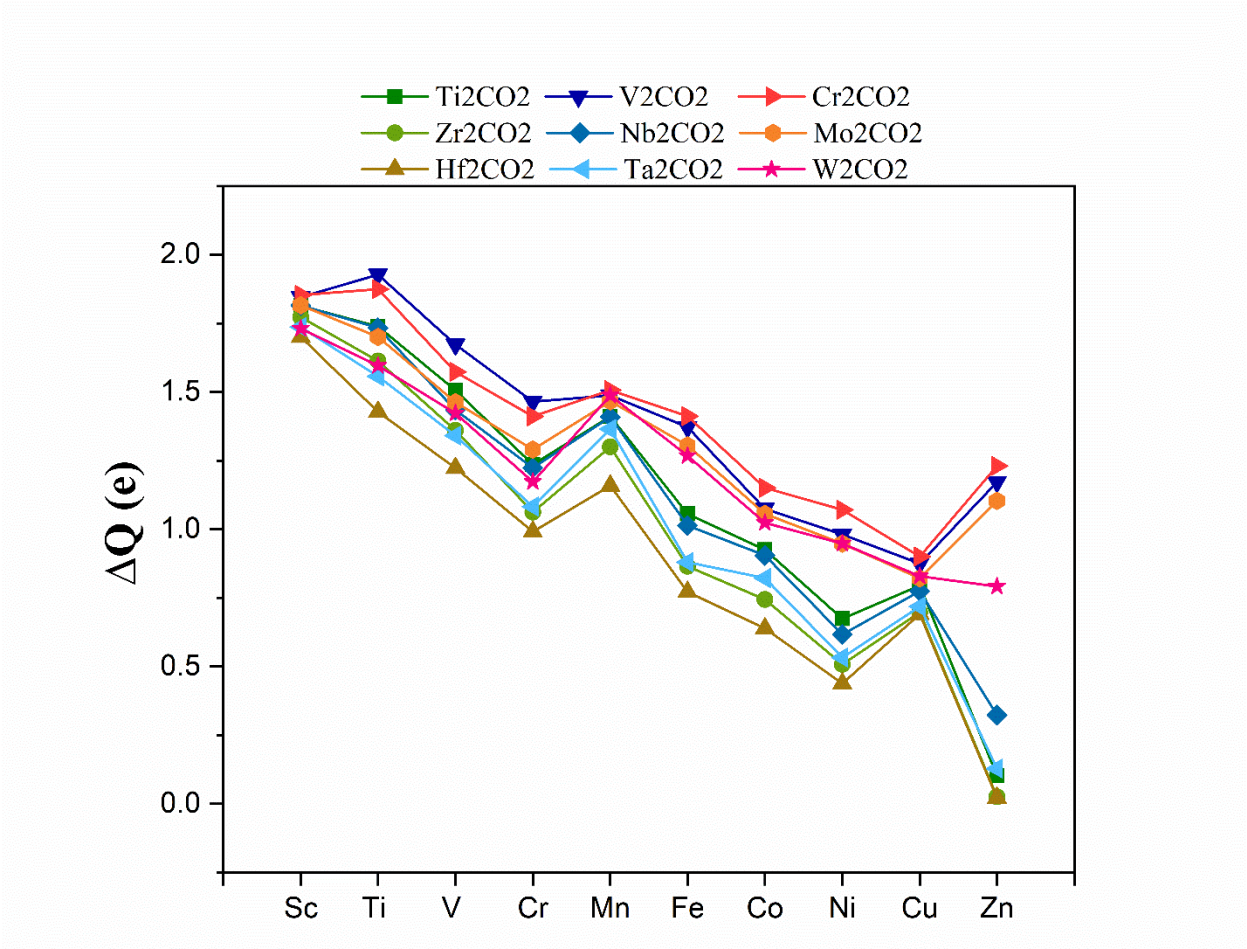

Fig. 4 Vertical distance (*h*) between the TM adatom and the O-terminated MXene surface. These results correspond to the most favorable situations at PBE-D3 connecting with those reported in Figs. 1 and 2.

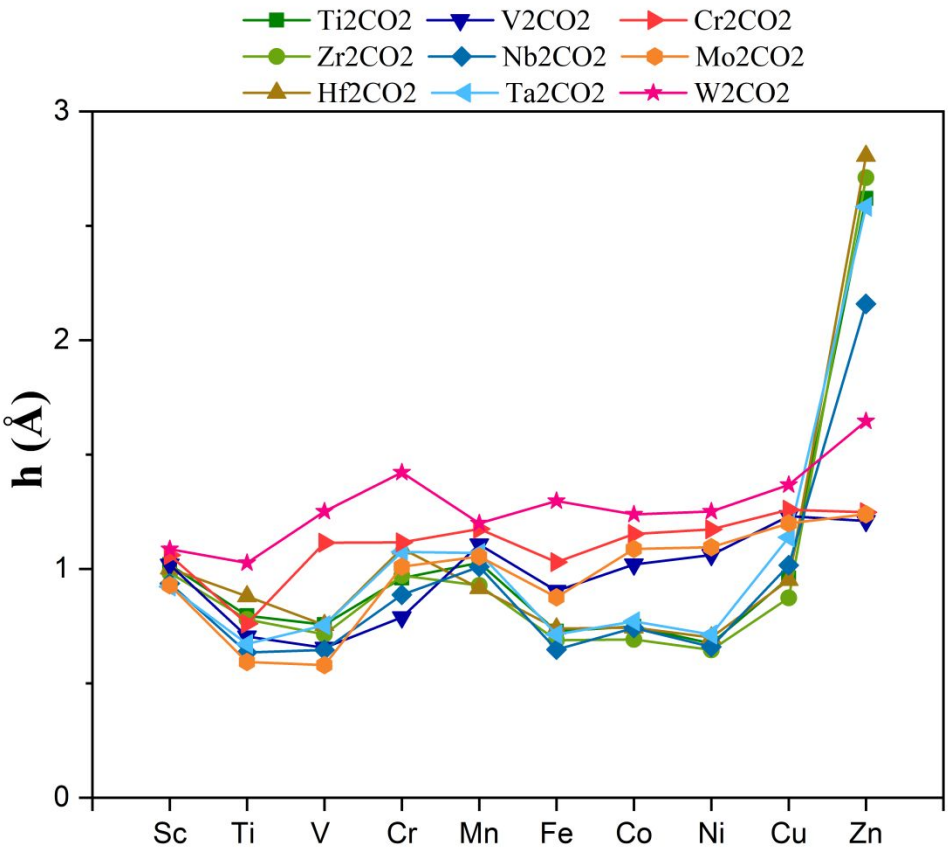

Fig. 5 Trends of E_{ads} (TM@M_2CO_2) versus the Bader charge on the TM adatom. The most favorable interactions are considered in both CABCA and BABCB MXenes.

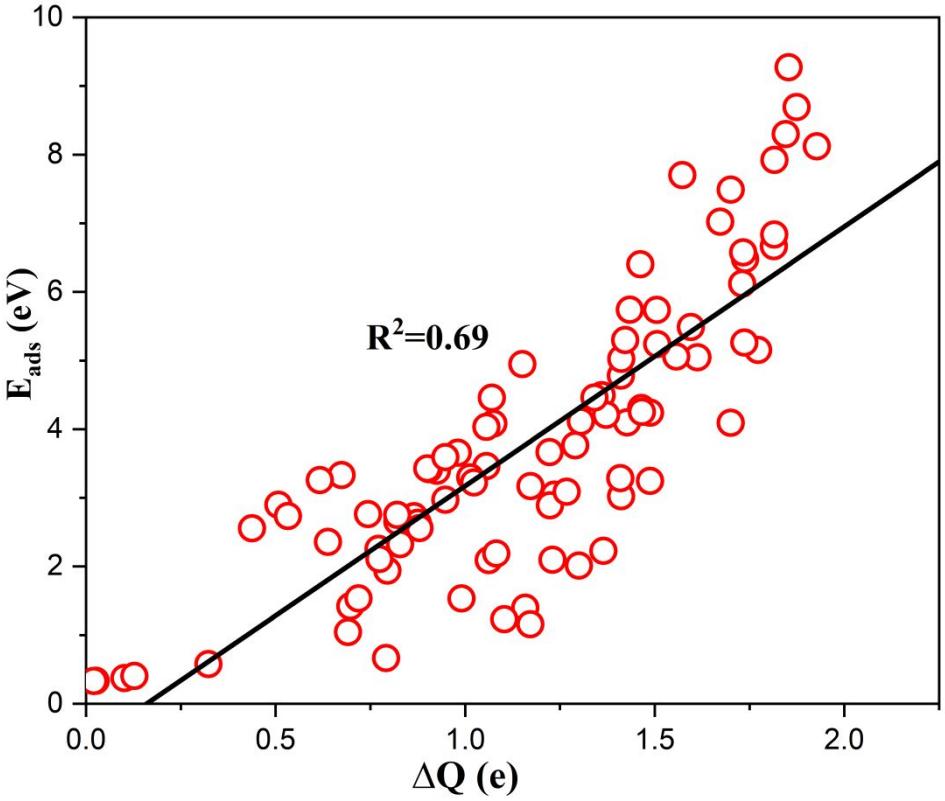

Fig. 6 Possible diffusion paths for TM adatoms through the (0001) surface of O-terminated MXenes with CABCA (left) and BABCB (right) stacking. Three different routes are explored moving from hollow-to-hollow sites.

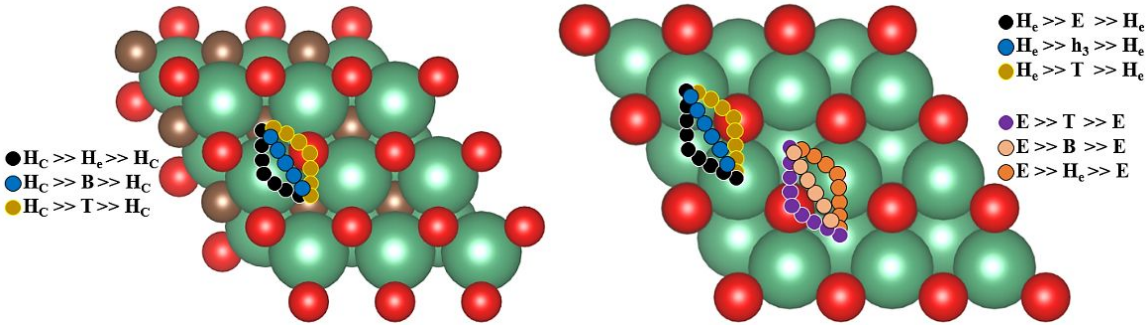

Fig. 7 Trends of E_{ads} (TM@M_2C) vs. E_{ads} (TM@M_2CO_2). The most favorable interactions are considered in both MXenes.

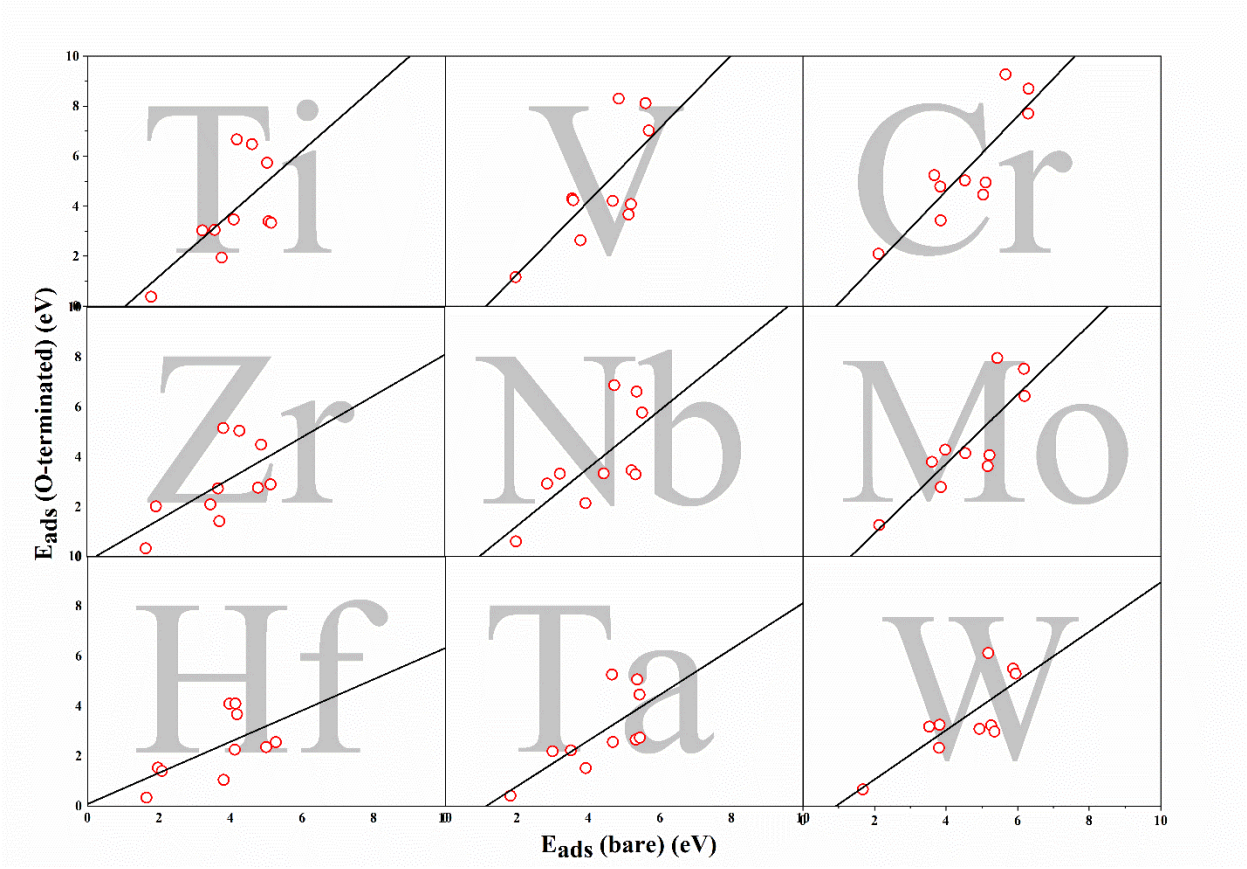

Table 1. E_{diff} (in eV) defined as the difference between E_{ads} and E_{coh} of all TM@M_2CO_2. By definition $E_{diff} > 0$ (marked in bold) indicates the energetic stabilization of single atom (isolating). Contrary $E_{diff} < 0$ favors agglomeration of TM adatoms (clustering).

MXene	**Adatoms**									
	Sc	**Ti**	**V**	**Cr**	**Mn**	**Fe**	**Co**	**Ni**	**Cu**	**Zn**
Ti_2CO_2	**2.17**	**0.62**	-0.68	-1.56	-1.21	-1.69	-2.17	-1.88	-1.90	-1.09
Zr_2CO_2	**0.72**	-0.75	-1.88	-2.39	-2.19	-2.39	-2.77	-2.28	-2.38	-1.09
Hf_2CO_2	-0.32	-1.68	-2.69	-2.88	-2.79	-2.86	-3.21	-2.63	-2.76	-1.09
V_2CO_2	**3.77**	**2.22**	**0.57**	-0.34	-0.01	-1.06	-1.52	-1.59	-1.22	-0.31
Nb_2CO_2	**2.20**	**0.60**	-0.80	-1.54	-1.08	-1.94	-2.28	-2.04	-1.84	-1.06
Ta_2CO_2	**0.79**	-0.78	-1.94	-2.30	-2.01	-2.60	-2.95	-2.49	-2.32	-1.09
Cr_2CO_2	**4.67**	**2.70**	**1.15**	**0.41**	**0.92**	-0.30	-0.80	-0.92	-0.52	**0.56**
Mo_2CO_2	**3.35**	**1.51**	-0.09	-0.60	-0.04	-1.19	-1.70	-1.79	-1.21	-0.29
W_2CO_2	**1.64**	-0.35	-1.07	-1.31	-0.98	-2.16	-2.37	-2.27	-1.53	-0.81

Table 2. Diffusion barriers, E_{bar} (in eV) of TM adatoms on MXenes. These results correspond to the most favorable situations at PBE-D3 connecting with those reported in Figs. 1 and 2. Values in bold corresponds to E_{bar} above 1.30 eV.

MXene	**TM adatoms**									
	Sc	**Ti**	**V**	**Cr**	**Mn**	**Fe**	**Co**	**Ni**	**Cu**	**Zn**
Ti_2CO_2	**1.55**	**1.60**	**1.38**	0.38	0.57	0.86	0.73	0.82	0.28	0.03
Zr_2CO_2	**1.44**	**1.66**	**1.50**	0.54	0.61	1.15	0.96	1.20	0.59	0.02
Hf_2CO_2	1.15	**1.39**	**1.33**	0.47	0.51	1.14	0.91	1.14	0.42	0.03
V_2CO_2	**1.36**	**1.74**	1.20	1.26	0.55	**1.34**	0.63	0.44	0.11	0.29
Nb_2CO_2	1.26	**1.49**	0.97	0.27	0.44	0.31	0.38	0.37	0.03	0.14
Ta_2CO_2	1.18	**1.48**	0.73	0.11	0.36	0.56	0.39	0.52	0.11	0.02
Cr_2CO_2	**1.44**	**2.00**	0.98	0.33	**1.53**	0.43	**1.30**	1.23	0.16	0.71
Mo_2CO_2	1.19	**1.61**	0.89	0.25	0.45	0.40	0.47	0.34	0.10	0.43
W_2CO_2	0.97	0.91	0.56	0.12	0.35	0.30	0.32	0.17	0.09	0.09

REFERENCES

(1) B. Qiao, A. Wang, X. Yang, L. F. Allard, Z. Jiang, Y. Cui, J. Liu, J. Li, and T. Zhang. Single-Atom Catalysis of Co Oxidation Using Pt_1/FeO_x. *Nat. Chem.*, 2011, **3**, 634.

(2) A. Wang, J. Li and T. Zhang. Heterogeneous Single-Atom Catalysis. *Nat. Rev. Chem.*, 2018, **2**, 65.

(3) X. Su, X. F. Yang, Y. Huang, B. Liu, and T. Zhang. Single-Atom Catalysis Towards Efficient CO_2 Conversion to CO and Formate Products. *Acc. Chem. Res.* 2019, **52**, 656.

(4) J. Li, M. F. Stephanopoulos and Y. Xia. Introduction: Heterogeneous Single-Atom Catalysis. *Chem. Rev.* 2020, **120**, 11699-11702.

(5) S. Mitchell and J. Pérez-Ramírez. Single Atom Catalysis. A Decade of Stunning Progress and the Promise for a Bright Future. *Nat. Commun.*, 2020, **11**, 4302.

(6) B. Bayatsarmadi, Y. Zheng, A. Vasileff, and S. Qiao. Recent Advances in Atomic Metal Doping of Carbon-Based Nanomaterials for Energy Conversion. *Small*, 2017, **13**, 1700191.

(7) J. Kim, H. Kim, and H. Lee. Single-Atom Catalysts of Precious Metals for Electrochemical Reactions. *ChemSusChem*, 2018, **11**, 104-113.

(8) S. Liang, C. Hao, and Y. Shi. The Power of Single-Atom Catalysis. *ChemCatChem*, 2015, **7**, 2559-2567.

(9) L. Liu and A. Corma. Metal Catalyst for Heterogeneous Catalysis: From Single Atoms to Nanoclusters and Nanoparticles. *Chem. Rev.*, 2018, **118**, 4981-5079.

(10) X.-F. Yang, A. Wang, B. Qiao, J. Li, J. Liu, and T. Zhang. Single-Atom Catalysts: A New Frontier in Heterogeneous Catalysis. *Acc. Chem. Res.*, 2013, **46**, 1740-1748.

(11) J. Li, L. Sun, Q. Wan, J. Lin, S. Lin and X. Wang. α-MoC Supported Noble Metal Catalysts for Water-Gas Shift Reaction: Single-Atom Promoter or Single-Atom Player. *J. Phys. Chem. Lett.*, 2021, **12**, 11415-11421.

(12) J. Li, L. Zhang, K. Doyle-Davis, R. Li and X. Sun. Recent Advances and Strategies in the Stabilization of Single-Atom Catalysts for Electrochemical Applications. *Carbon Energy*, 2020, **2**, 488-520.

(13) A. Sara, C. A. Salai and H. Andrea. On the Importance of Metal-Oxide Interface Sites for the Water-Gas Shift Reaction over Pt/CeO_2 Catalysts. *J. Catal.*, 2014, **309**, 314-324.

(14) G. Gao, Y. Jiao, E. R. Waclawik and A. Du. Single Atom (Pd/Pt) Supported on Graphitic Carbon Nitride as An Efficient Photocatalysts for Visible-Light Reduction of Carbon Dioxide. *J. Am. Chem. Soc.*, 2016, **138**, 6292-6297.

(15) G. Xiang-Kui, Q. Botao, H. Chuan-Qi, D. Wu-Chen, S. Keju, Z. Ensheng, Z. Tao, L. Jingyue and L. Wei-Xue. Supported Single Pt_1/Au_1 Atoms for Methanol Steam Reforming. *ACS Catal.*, 2014, **4**, 3886-3890.

(16) X. P. Guang, Y. L. Xiao, Y. Xiaofeng, Z. Leilei, W. Aiqin, L. Lin, W. Hua, W. Xiaodong and Z. Tao. Performance of Cu-Alloyed Pd Single-Atom Catalyst for Semihydrogenation of Acetylene Under Simulated Front-End Conditions. *ACS Catal.*, 2017, **7**, 1491-1500.

(17) X. Guang, X. P. Pei, L. Meng, C. Qian, w. Aiqin and Z. Tao. Isolation of Pd Atoms by Cu for Semi-Hydrogenation of Acetylene: Effects of Cu Loading. *Chi. J. Catal.*, 2017, **38**, 1540-1548.

(18) S. Sun, G. Zhang, n. Gauquelin, N. Chen, J. Zhou, S. Yang, W. Chen, X. Meng, D. Geng, M. N. Banis, R. Y. Li, S. Y. Ye, S. Knights, G. A. Botton, T. K. Sham, and X. L. Sun. Single-Atom Catalysis Using Pt/Graphene Achieved through Atomic Layer Depostion. *Sci. Rep.*, 2013, **3**, 1775.

(19) Z. Luo, Y. Ouyang, H. Zhang, M. Xiao, J. Ge, Z. Jiang, J. Wang, D. Tang, X. Cao, C. Liu and W. Xing. Chemically Activating MoS_2 via Spontaneous Atomic Palladium Interfacial Doping towards Efficient Hydrogen Evolution. *Nat. Commun.*, 2018, **9**, 2120.

(20) J. Zhang, J. Liu, L. Xi, Y. Yu, N. Chen, S. Sun, W. Wang, K. M. Lange and B. Zhang. Single-Atom Au/NiFe Layered Double Hydroxide Electrocatalyst: Probing the origin of Activity for oxygen Evolution Reaction. *J. Am. Chem. Soc.*, 2018, **140**, 3876-3879.

(21) B. Anasori, M. R. Lukatsaya, Y. Gogotsi. 2D Metal Carbides and Nitrides (MXenes) for Energy Storage. *Nat. Rev. Mater.* 2017, **2**, 16098.

(22) Á. Morales-García, F. Calle-Vallejo and F. Illas. MXenes: New Horizons in Catalysis. *ACS Catal.*, 2020, **10**, 13487-13503.

(23) D. Zhao, Z. Chen, W. Yang, S. Liu, X. Zhang, Y. Yu, W. C. Cheong, L. Zheng, R. Fen, G. Ying, X. Cao, D. Wang, Q. Peng, G. Wang and C. Chen. MXene (Ti_3C_2) Vacancy-Confined Single-Atoms Catalyst for Efficient Functionalization of CO_2. *J. Am. Chem. Soc.*, 2019, **141**, 4086-4093.

(24) J. Zhang, Y. Zhao, X. gou, C. Chen, C. L. Dong, R. S. Liu, c. P. Han, Y. Li, Y. Gogotsi and G. Wang. Single Platinum Atoms Immobilized on an MXene as an efficient Catalyst for the Hydrogen evolution Reaction. *Nat. Catal.*, 2018, **1**, 985-992.

(25) H. Oschinski, Á. Morales-García and F. Illas. Interaction of First Row Transition Metals with M_2C (M=Ti, Zr, Hf, V, Nb, Ta, Cr, Mo, and W) MXenes: A Quest for Single-Atom Catalysts. *J. Phys. Chem. C,* 2021, **125**, 2477-2484.

(26) M. Alhabed, K. Maleski, B. Anasori, P. Lelyukh, L. Clark, S. Sin and Y. Gogotsi. Guidelines for Synthesis and Processing of Two-Dimensional Titanium Carbide ($Ti_3C_2T_x$ MXene). *Chem. Mater.*, 2017, **29**, 7633-7644.

(27) M. Naguib, M. W. Barsoum and Y. Gogotsi. Ten Years of Progress in the Synthesis and Development of MXenes. *Adv. Mater.*, 2020, 2103393 (Early View)

(28) I. M. Chirica, A. G. Mirea, S. Neatu, M. Florea, M. W. Barsoum, F. Neatu, Applications of MAX phases and MXenes as catalysts. *J. Mater. Chem. A*, 2021, **9**. 19589-19612

(29) X. Zhang, B. Shao, Z. Sun, Z. Gao, Y. Qin, C. Zhang, F. Cui and X. Yang. Platinum Nanoparticle-Deposited $Ti_3C_2T_x$ MXene for Hydrogen Evolution Reaction. *Ind. Eng. Chem. Res.*, 2020, **59**, 1822-1828.

(30) C. Ling, L. Shi, Y. Ouyang and J. Wang. Transition Metal-Promoted V_2CO_2 (MXenes): A New and Highly Active Catalyst for Hydrogen Evolution Reaction. *Adv. Sci.*, 2016, **3**, 1600180.

(31) Y. Cheng, J. Dai, Y. Song and Y. Zhang. Nanostructure of Cr_2CO_2 MXene Supported Single Metal Atom as an Efficient Bifunctional Electrocatalyst for Overall Water Splitting. *ACS Appl. Energy Mater.*, 2019, **2**, 6851-6859.

(32) L. M. Azofra, N. Li, D. R. MacFarlane and C. Sun. Promising Prospect for 2D d^2-d^4 M_3C_2 Transition Metal Carbides (MXenes) in N_2 Capture and Conversion into Ammonia. *Energy Environ. Sci.*, 2016, **9**, 2545-2549.

(33) Y. Guo, T. Wang, Q. Yang, X. Li, H. Li, Y. Wang, T. Jiao, Z. Huang, B. Dong, W. Zhang, J. Fan and C. Zhi. Highly Efficient Electrochemical Reduction of Nitrogen to Ammonia on Surface termination Modified $Ti_3C_2T_x$ MXene Nanosheets. *ACS Nano*, 2020, **14**, 9089-9097.

(34) X. Yang, Y. Zhang, Z. Fu, Z. Lu, X. Zhang, Y. Wang, Z. Yang and R. Wu. Tailoring the Electronic Structure of Transition Metals by the V_2C MXene Support: Excellent Oxygen

Reduction Performance Triggered by Metal-Support Interactions. *ACS Appl. Mater. Interfaces*, 2020, **12**, 28206-28216.

(35) J. D. Gouveia, Á. Morales-García, F. Viñes, F. Illas and J. R. B. Gomes. MXenes as Promising Catalysts for Water Dissociation. *Appl. Catal. B Environ.*, 2020, **260**, 118191.

(36) J. D. Gouveia, Á. Morales-García, F. Viñes, J. R. B. Gomes and F. Illas. Facile Heterogeneously Catalyzed Nitrogen Fixation by MXenes. *ACS Catal*., 2020, **10**, 5049-5056.

(37) R. Morales-Salvador, J. D. Gouveia, Á. Morales-García, F. Viñes, J. R. B. Gomes and F. Illas. Carbon Capture and Usage by MXenes. *ACS Catal.*, 2021, **11**, 11248-11255.

(38) J. A. Rodriguez, F. Illas. Activation of Noble Metals on Metal-Carbide Surfaces: Novel Catalysts for CO Oxidation, Desulfurization and Hydrogenation Reactions. *Phys. Chem. Chem. Phys.* 2012, **14**, 427-438.

(39) T. Gómez, E. Florez, J. A. Rodriguez and F. Illas. Theoretical analysis of the adsorption of late transition metal atoms on the (001) surface of early transition metal carbides. *J. Phys. Chem. C*, 2010, **114**, 1622-1626.

(40) H. Prats, R. A. Gutiérrez, J. J. Piñero, F. Viñes, S. T. Bromley, P. J. Ramírez, J. A. Rodriguez, F. Illas. Room Temperature Methane Capture and Activation by Ni Clusters Supported on TiC(001): Effects of Metal-Carbide Interactions on the Cleavage of the C-H Bond. *J. Am. Chem. Soc.* 2019. **141**, 5303-5313.

(41) J. Zhang, Y. Zhao, X. Guo, C. Chen, C.-L. Dong, R.-S. Liu, C.-P. Han, Y. Li, Y. Gogotsi and G. Wang. Single Platinum Atoms Immobilized on an MXene as an Efficient Catalyst for the Hydrogen Evolution Reaction. *Nat. Catal.*, 2018, **1**, 985-992.

(42) X. Yang, Z. Lu, C. Cheng, Y. Wang, X. Zhang, Z. Yang and W. Lu. Identification of Efficient Single-Atom Catalysts Based on V_2CO_2 MXene by *Ab Initio* Simulations. *J. Phys. Chem. C*, 2020, **124**, 4090-4100.

(43) J. Qu, J. Xiao, H. Chen, X. Liu, T. Wang and Q. Zhang. Orbital Symmetry Matching: Achieving Superior Nitrogen Reduction Reaction Over Single-Atom Catalysts Anchored on MXene Substrates. *Chin. J. Catal.*, 2021, **42**, 288-296.

(44) Y.-H. Chen, M-Y. Qi, Y.-H. Li, Z.-R. Tang, T. Wang, J. Gong, Y.-J. Xu. Activating two-dimensional $Ti_3C_2T_x$-MXene with Single-Atom Cobalt for Efficient CO_2 Photoreduction. *Cell Reports Phys. Sci.*, 2021, **2**, 100371.

(45) Y. Gao, Y. Cao, Y. Gu, H. Zhuo, G. Zhuang, S. Deng, X. Zhong, Z. Wei, J. Chen, X. Pan and J.-G. Wang. Functionalization Ti_3C_2 MXene by the Adsorption or Substitution of Single Metal Atom. *Appl. Surf. Sci.*, 2019, **465**, 911-918.

(46) E. B. Deeva, A. Kurlov, P. M. Abdala, D. Lebedev, S. M. Kim, C. P. Gordon, A. Tsoukalou, A. Fedorov and C. R. Müller. In Situ XANES/XRD Study of the Structural Stability of Two-Dimensional Molybdenum Carbide Mo_2CT_x: Implications for the Catalytic Activity in the Water-Gas Shift Reaction. *Chem. Mater.* 2019, **31**, 4505-4513.

(47) V. Kamysbayev, A. S. Filatov, H. Hu, X. Rui, F. Lagunas, D. Wang, R. F. Klie, D. V. Talapin. Covalent surface modifications and superconductivity of two-dimensional metal carbide MXenes. *Science* **2020**, *369*, eaba8311.

(48) G. Kresse and J. Furthmüller. Efficient iterative schemes for ab initio total-energy calculations using a plane-wave basis set. *Phys. Rev. B*, 1996, **54**, 11169.

(49) G. Kresse and J. Furthmüller. Efficiency of ab-initio total energy calculations for metals and semiconductors using a plane-wave basis set. *Comput. Mater. Sci.*,1996, **6**, 15–50.

(50) P. E. Blöchl. Projector augmented-wave method. *Phys. Rev. B*, 1994, **50**, 17953.

(51) H. J. Monkhorst and J. D. Pack. Special points for Brillouin-zone integrations. *Phys. Rev. B*, 1976, **13**, 5188.

(52) J. P. Perdew, K. Burke and M. Ernzerhof. Generalized gradient approximation made simple. *Phys. Rev. Lett.*, 1996, **77**, 3865.

(53) S. Grimme, J. Antony, S. Ehrlich and H. Krieg. A consistent and accurate ab initio parametrization of density functional dispersion correction (DFT-D) for the 94 elements H-Pu. *J. Chem. Phys.*, 2010, **132**, 154104.

(54) N. García-Romeral, M. Keyhanian, Á. Morales-García and F. Illas. Relating X-Ray Photoelectron Spectroscopy Data to Chemical Bonding in MXenes. *Nanoscale Adv.*, 2021, **3**, 2793-2801.

(55) Janthon, P.; Kozlov, S. M.; Viñes, F.; Limtrakul, J.; Illas, F. Establishing the Accuracy of Broadly Used Density Functional in Describing Bulk Properties of Transition Metals. *J. Chem. Theory Comput.* **2013**, *9*, 1631-1640.

(56) R. F. W. Bader. *Atoms in Molecules: A Quantum Theory, International Series of Monographs on Chemistry*. (Clarendon Press, Oxford, 1994)

(57) Y. Zhang, X.-H. Zha, K. Luo, N. Qiu, Y. Zhou, J. He, Z. Chai, Z. Huang, Q. Huang, Y. Liang and S. Du. Tuning the Electrical Conductivity of Ti_2CO_2 MXene by Varing the Layer Thickness and Applying Strains. *J. Phys. Chem. C*, 2019, **123**, 6802-6811.

(58) S. Wang, L. Li, K. S. Hui, F. Bin, W. Zhou, X. Fan, E. Zalnezhad, J. Li and K. N. Hui. Computational Screening of Single Atoms Anchored on Defective Mo_2CO_2 MXene Nanosheet as Efficient Electrocatalysts for the Synthesis of Ammonia. *Adv. Eng. Mater.*, 2021, 2100405.

(59) Z. Tan, Z. Fang, B. Li and Y. Yang. First-Principles Study of the Ferromagnetic Properties of Cr_2CO_2 and Cr_2NO_2. *ACS Omega*, 2020, **5**, 25848-25853.

(60) Gouveia, J. D.; Viñes, F.; Illas, F.; Gomes, J. R. B. MXenes Atomic Layer Stacking Phase Transitions and Their Chemical Activity Consequences. *Phys. Rev. Mater.* **2020**, *4*, 054003.

(61) A. Jurado, Á, Morales-García, F. Viñes, F. Illas. Identifying the Atomic Layer Stacking of Mo2C MXene by Probe Molecule Adsorption. J. Phys. Chem. C, in press, DOI: https://doi.org/10.1021/acs.jpcc.1c07577.

(62) M. Manadé, F. Viñes and F. Illas. Transition Metal Adatoms on Graphene: A Systematic Density Functional Study. *Carbon*, 2015, **95**, 525-534.

(63) S. Kim, A. R. Puigdollers, P. Gamallo, F. Viñes and J. Y. Lee. Functionalization of γ-graphyne by Transition Metal Adatoms. *Carbon*, 2017, **120**, 63-70.

(64) D. Kan, D. Wang, Y. Cheng, R. Lian, B. Sun, K. Chen, W. Huo, Y. Wang, G. Chen and Y. Wei. Designing of Efficient Bifunctional ORR/OER Pt Single-Atom Catalysts Based on O-terminated MXenes by First-Principles Calculations. *ACS Appl. Mater. Interfaces*, 2021, **13**, 52508-52518.

(65) D. Kan, D. Wang, Y. Cheng, R. Lian, B. Sun, K. Chen, W. Huo, Y. Wang, G. Chen and Y. Wei. Designing of Efficient Bifunctional ORR/OER Pt Single-Atom Catalysts Based on O-terminated MXenes by First-Principles Calculations. *ACS Appl. Mater. Interfaces*, 2021, **13**, 52508-52518.

(66) B. Cai, J. Zhou, D. Li and Z. Ao. New Insights into the Single-Atom-Decorated Zr_2CO_2 (MXene) as an Efficient Catalyst for CO Oxidation in Incomplete Combustion Gas. *Appl. Surf. Sci.*, 2022, **575**, 151777.

TOC